Available online at www.sciencedirect.com
SCIENCE DIRECT®
Cold Regions Science and Technology 43 (2005) 24–35
cold regions science and technology
www.elsevier.com/locate/coldregions

On size and shape effects in snow fracture toughness measurements

Christian Sigrist[a,*], Jürg Schweizer[a], Hans-Jakob Schindler[b], Jürg Dual[c]

[a]WSL, Swiss Federal Institute for Snow and Avalanche Research SLF, Flüelastrasse 11, CH-7260 Davos Dorf, Switzerland
[b]Mat-Tec AG, Unterer Graben 27, CH-8401 Winterthur, Switzerland
[c]Institute of Mechanical Systems, ETH Zürich, Swiss Federal Institute of Technology, CH-8092 Zürich, Switzerland

Received 11 September 2004; accepted 11 January 2005

Abstract

Dry snow slab avalanche release is preceded by two fracture mechanical processes: shear failure of a weak layer or an interface within the snowpack, followed by tensile failure of the overlaying slab. For a slope stability analysis based on fracture mechanics, the fracture toughness of snow has to be known. The purpose of this work was to evaluate snow fracture toughness in mode I, to determine to what extent it is affected by the specimen size and shape and to search for adequate correction methods. Edge-cracked beam-shaped snow specimens cut from homogeneous layers of naturally deposited snow were subjected to three-point bending and cantilever beam tests. To describe the size dependence an empirical size effect law and the FAD (failure assessment diagram) approach were explored. By comparing the three-point bending with the cantilever beam tests a shape dependence of the toughness was found. The fracture process zone was estimated to be in the order of at least one centimetre. Due to the large size of the fracture process zone a dependence of the toughness on the specimen size has to be expected, as it is typical for non-linear, quasi-brittle materials. Experiments with four different specimen sizes clearly confirmed that toughness is size dependent, possibly up to the scale of a slab avalanche. Preliminary results suggest that the actual fracture toughness might be twice as large as the one determined experimentally. Therefore, size correction functions will be essential to transform toughness data of laboratory-scaled experiments to the scale relevant for snow slope stability models.

Keywords: Snow fracture toughness; Snow mechanics; Fracture mechanics; Avalanche formation; Size effect; Shape effect

1. Introduction

Before the release of a dry snow slab avalanche several damage processes occur. Damage accumulation in a weak layer of the snowpack or along an interface between two different snow layers leads to an initial failure in shear followed by fractures in tension, which finally releases the slab avalanche (Perla and LaChapelle, 1970, Schweizer et al., 2003). Both fracture processes can be described and understood by the theory of fracture mechanics. Thus, the corresponding material characteristics such

* Corresponding author. Tel.: +41 81 417 0175; fax: +41 81 417 0110.
E-mail address: sigrist@slf.ch (C. Sigrist).

0165-232X/$ - see front matter © 2005 Elsevier B.V. All rights reserved.
doi:10.1016/j.coldregions.2005.05.001

as the fracture toughness in Mode I and Mode II have to be known (McClung, 1981). They are essential to well-founded and reliable slab release models.

The available data on fracture toughness of snow are still relatively few (Kirchner et al., 2000; Kirchner et al., 2002a,b; Faillettaz et al., 2002; and Schweizer et al., 2004). In all previous studies cantilever beam tests were used to determine fracture toughness. Assuming linear elastic fracture mechanics (LEFM) to be applicable, they obtained K_{Ic} values ranging from 0.1 to 1.5 kPa $m^{1/2}$, depending on snow type and density. However, Schweizer et al. (2004) pointed out that the standard size requirements for LEFM were not fulfilled for the specimens used ($20 \times 50 \times 10$ cm), which makes the application of the test results to snow slope stability models questionable.

Bazant et al. (2003) related fracture toughness to the avalanche release process by taking a size effect into account. They formulated a size effect law based on equivalent linear elastic fracture mechanics and found that fracture toughness in shear is approximately proportional to the thickness of the overlaying slab to the power of 1.8. Dempsey et al. (1999a,b) tested sea ice over a very large sample range from 0.1 up to 100 m and confirmed Bazant's empirical size effect law (Bazant and Planas, 1998) to be valid even over this large range. They calibrated the size effect law with experiments between 0.1 and 3 m and were then able to predict correct toughness values up to a size of 100 m.

The present paper introduces a new test method and reports on a preliminary study on the size and shape dependence of snow fracture toughness and on possibilities for corresponding corrections. The final aim is to extrapolate laboratory toughness data to the snow slab avalanche scale. For this purpose four different specimen sizes and three different specimen geometries were used: two types of cantilever beam tests with different protrusion, and a three-point bending test. Furthermore, attempts were made to estimate the size of the nonlinear fracture process zone.

However, regarding the variety of influencing parameters, the presented experimental data are not yet statistically sound. They have to be considered as preliminary and need to be confirmed by further tests.

2. Experimental methods

2.1. Three-point bending test

Three-point bending tests (3PB-tests) were performed on snow samples of naturally deposited snow with a standard testing apparatus (Fig. 1). The specimens were cut out of the snowpack in the surroundings of Davos (Switzerland) with beam-shaped aluminium cases. The density of the snow samples ranged from 140 to 380 kg/m^3. Four different sizes of cases were used (Table 1). The largest snow case was close to the limit of what can be handled in the field and transported to the laboratory without destroying the natural snow structure. The other sizes were chosen such that a size range of 1:4 was achieved and included the one used by Schweizer et al. (2004) ($20 \times 50 \times 10$ cm). The thickness w was the same for all specimen sizes in order to avoid a possible thickness effect ("2D similarity", according to Bazant and Planas (1998)).

All experiments were performed in the SLF cold laboratories at Weissfluhjoch and Davos (Switzerland) at temperatures between -7 and -15 °C in a standard material testing apparatus which is designed to measure compressive or tensile forces up to 20 kN with a resolution of 0.1 N. The snow specimens were supported by two aluminium cylinders with a diameter of 6 cm separated by a span s (Fig. 2a). Into the central cross section, a sharp cut of variable length a was introduced from below with a thin metal saw blade. The load was applied in

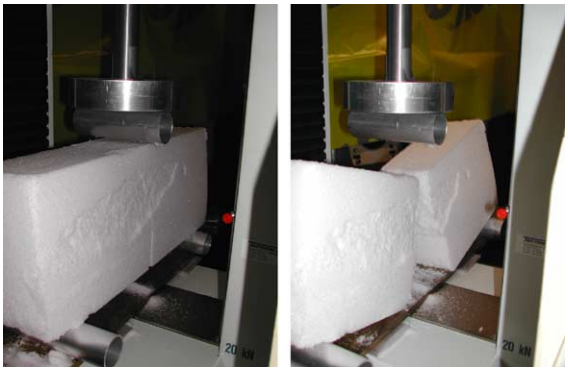

Fig. 1. Three-point bending setup before and after cracking. Snow specimen dimension: $20 \times 50 \times 10$ cm.

Table 1
Snow specimen dimensions used to determine the size effect (Series E, Table 2)

Height h (cm)	Length l (cm)	Width w (cm)
8	20	10
13	31	10
20	50	10
32	80	10

displacement control at a constant rate of 200 mm/min through another aluminium cylinder with a diameter of 5 cm. The velocity was chosen high in order to cause a brittle fracture and to avoid viscous effects. The aluminium cylinders were used to increase the contact area and thus to prevent local snow deformation at the loading points. The diameter of the cylinders is expected to have only a minor influence on the test results.

The force required to break the specimens, F_c, was small and ranged between 1 and 60 N, depending on beam size and density. Thus, the weight of the beam had to be taken into account in calculating the applied stress and stress intensity factor.

The stress intensity factor (SIF) for the present system can be obtained by combining the 3PB-solution and the pure bending case given by Tada et al. (2000). Correspondingly, the critical stress intensity factor K_{IQ}, which is defined as the fracture toughness K_{Ic} if the size criterion for LEFM turns out to be fulfilled, is obtained as:

$$K_{IQ} = \sqrt{\pi a}\frac{6}{h^2}\left[0.95\frac{F_c s}{4w} f_1\left(\frac{a}{h}\right) + M_m f_2\left(\frac{a}{h}\right)\right] \quad (1)$$

where a is the crack or cut length and h the specimen height. The functions $f_1(a/h)$ and $f_2(a/h)$ are given in Tada et al. (2000). The factor 0.95 in the first term was found in a numerical computation to be appropriate to correct for the difference in the ratio s/h between the experiments (s/h between 2 and 2.5) and the SIF-solution in Tada et al. (2000) ($s/h=4$). M_m is the moment per beam width due to the body weight:

$$M_m = \frac{1}{8}\left(\frac{G_{3PB}}{s}\right)\left[s^2 - (l-s)^2\right] \quad (2)$$

where $G_{3PB}=sh\rho g$. s is the span of the specimen, w its width, l its length, ρ the snow density and g the acceleration of gravity (Fig. 2a). For our 3PB-experiments the part due to the moment M_m in Eq. (1), is about 60% of the part due to the force ($F_c s/4w$).

2.2. Cantilever beam test

In order to link the experimental data to those of Schweizer et al. (2004) the same cantilever beam tests (CB-tests) were performed. The specimens were notched from top until the protruding part with length L broke off under its own weight at a critical cut length $a=a_c$ (Fig. 2b). L was chosen to be either 10 cm or 15 cm. Since the cut in the CB-tests is loaded in mixed mode, the SIF in mode II, K_{II}, has to be taken into account. For $h-a<L$, the system is equivalent to the asymptotic case of a deep edge crack under a bending moment and a shear force. The corresponding SIF are given in Tada et al. (2000):

$$K_I = \frac{3.975M}{(h-a_c)^{3/2}} \quad (3)$$

and

$$K_{II} = \frac{1.463G_{CB}}{(h-a_c)^{1/2}} \quad (4)$$

where G_{CB} is the cantilever weight per specimen width ($G_{CB}=Lh\rho g$) and M is the moment per specimen width ($M=G_{CB}L/2$).

In a brittle material like snow, the mode interaction is likely to be governed by the criterion of maximum hoop stress suggested by Erdogan and Sih (1963),

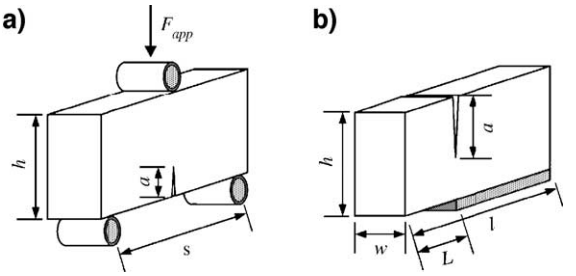

Fig. 2. Experimental setup for three-point bending test (a) and cantilever beam test (b).

which leads approximately to the following failure diagram (Schindler, 2004):

$$\left|\frac{K_{II}}{K_{Ic}}\right| \leq \frac{\sqrt{3}}{2}\sqrt{1-\frac{K_I}{K_{Ic}}}. \quad (5)$$

Replacing K_{Ic} in Eq. (5) by the critical SIF in Mode I, K_{IQ} yields:

$$K_{IQ} = \frac{K_I}{2} + \sqrt{\frac{K_I^2}{4} + \frac{4}{3}K_{II}^2}. \quad (6)$$

Eq. (6) slightly deviates from the formulation for the critical stress intensity factor given by Kirchner et al. (2002a). Particularly for deep cuts, Eq. (6) is the more appropriate approximation. Taking K_{II} into account in Eq. (6) increases K_{IQ} by about 6% to 37%, depending on snow density.

3. Size requirement

In the presence of a crack, a local non-linear zone evolves in any material due to the extreme stress concentration at the crack-tip. As long as the length R_c of this non-linear zone remains small compared to the crack length and the characteristic dimensions of the specimen, LEFM can still be applied (Anderson, 1995). In fracture toughness testing of elastic-plastic materials, the applicable standards like ASTM E399 require R_c at crack instability to be about 8 times smaller than the crack length a or the ligament width $h-a$, whichever is smaller. To estimate R_c, often Irwin's approximation of the plastic zone size is adapted (Irwin, 1958). By replacing the yield strength by the tensile strength of snow σ_{Rt}, the plastic zone at a crack-tip loaded in mode I can be expressed as:

$$R_c \cong \frac{1}{\pi}\left(\frac{K_I}{\sigma_{Rt}}\right)^2. \quad (7)$$

As snow is a non-ductile material at the strain rates applied in our tests, the non-linear zone is restricted to the fracture process zone at the crack-tip. In the fracture process zone the material behaviour is characterised by strain softening, i.e. decreasing stresses with increasing deformation. This behaviour can be described by Barenblatt's cohesive force model (Barenblatt, 1962). The strain-dependent strength of the material is interpreted as cohesive stresses $\sigma_{coh}(x)$ acting on virtual crack-faces in the range $0<x<R_c$, i.e. the process zone (Fig. 3). The distribution of $\sigma_{coh}(x)$ is usually unknown, but for physical reasons it has to be a decreasing function between the maximum at $x=R_c$ and zero at $x=0$. Assuming, for the sake of simplicity, $R_c \ll a$ and a linear behaviour of the cohesive stress with x, this model yields (Schindler, 1996):

$$R_c \cong \frac{9\pi}{32}\left(\frac{K_I}{\sigma_{Rt}}\right)^2, \quad (8)$$

which is about three times the value given by Eq. (7). Moreover, if the condition $R_c \ll a$ is not fulfilled, then R_c becomes dependent on the crack length and specimen geometry. Beyond LEFM, even Eq. (8) can considerably underestimate the actual length of the non-linear zone.

Concerning the size requirement which has to be fulfilled for an application of LEFM, there is only little experience on non-ductile materials in general and snow in particular. A simplified application of Barenblatt's model to a deeply cracked beam in bending (Schindler, 1996) indicates that the corresponding requirement should be at least as restrictive as the one given by ASTM E399 for elastic-plastic materials. The maximum length of the nonlinear zone is obtained from Eqs. (7) or (8), respectively, by setting $K_I=K_{Ic}$. In the case of sub-sized specimens, K_{Ic} is not known a priori, so it has to be replaced by K_{IQ}. Since

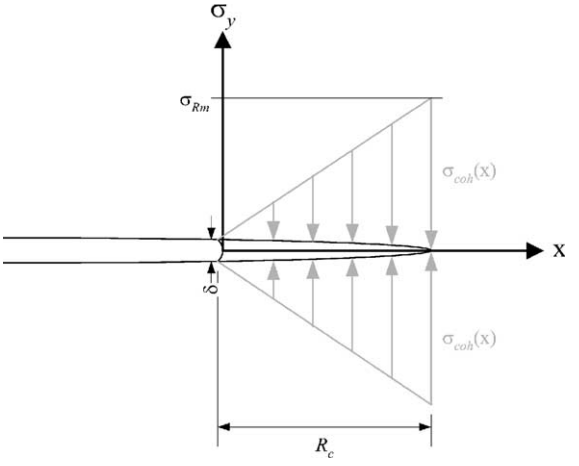

Fig. 3. Cohesive crack model with a linear distribution of the cohesive stresses $\sigma_{coh}(x)$ acting on the virtual crack-faces.

K_{IQ} is in general smaller than K_{Ic}, R_c can be significantly underestimated. To avoid this uncertainty it is preferable to use corrected K_{Ic} values in Eqs. (7) or (8) rather than K_{IQ} (see Section 4).

4. Size corrections and scaling laws

If LEFM does not apply, the fracture process is no longer governed by the stress intensity factors only. This means that the critical stress intensity factor K_{IQ} of Eq. (1) does not represent the actual fracture toughness K_{Ic} of the material, but an apparent fracture toughness that depends on the geometry and the size of the specimen. Thus the measured K_{IQ} values have to be corrected to the size of the problem which has to be solved.

4.1. Scaling law

Fracture processes that are governed by nominal stresses or plastic collapse are scalable, whereas those governed by crack instability are not (Bazant and Planas, 1998). The reason is that for a larger structure, more energy is released at the crack front by the same crack extension, Δa. Accordingly, there is no size effect in nominal strength σ_N for specimens which are smaller than a certain size. For large sizes a pure brittle behaviour is dominant and structures fail at a fixed stress intensity factor, which depends on the absolute crack length. This general behaviour is schematically shown in Fig. 4 (Bazant and Planas, 1998), using a general size parameter D.

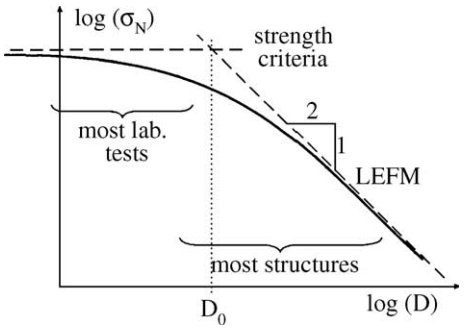

Fig. 4. Fracture mechanical size effect on the strength of a material (Bazant and Planas, 1998).

Based on experimental data of tensile fracture, Bazant and Planas (1998) proposed the following general scaling law for the nominal strength

$$\sigma_N = \frac{B\sigma_{Rt}}{\sqrt{1 + D/D_0}} \tag{9}$$

where σ_{Rt} is the tensile strength, B is a dimensionless constant, and D_0 a characteristic size. In Fig. 4, D_0 is the point where the line for linear elastic behaviour intersects with the horizontal line for plastic collapse. However, Eq. (9) can only serve to predict the size effect in cases of short cracks or geometrically similar crack systems.

4.2. Equivalent fracture toughness

According to Bazant and Planas (1998) it is possible to experimentally obtain an equivalent fracture toughness K_{Ic}^e which is an estimate of fracture toughness K_{Ic}. A simplified version of Eq. (1) is used, which neglects the factor 0.95 and replaces function f_2 with function f_1:

$$K_{IQ} = \sigma_N \sqrt{\pi a} f_1\left(\frac{a}{D}\right). \tag{10}$$

The nominal strength σ_N is defined as the maximum surface stress in the uncracked state

$$\sigma_N = \frac{6}{h^2}\left(\frac{F_c s}{4w} + M_m\right). \tag{11}$$

The error due to the simplification does not exceed 5% for our experiments and is justifiable for a first estimate of K_{Ic}^e. By rearranging Eq. (9) a linear dependence of the characteristic specimen size D is obtained:

$$\left(\frac{1}{\sigma_N}\right)^2 = c_1 D + c_2 \tag{12}$$

with $c_1 = \frac{1}{D_0 (B\sigma_{Rt})^2}$ and $c_2 = \frac{1}{(B\sigma_{Rt})^2}$.. In our experiments the characteristic length D is associated with the specimen height h. If the data are plotted as $\left(\frac{1}{\sigma_N}\right)^2$ versus the specimen height h, D_0 and $B\sigma_{Rt}$

can be estimated from slope and intercept of a linear regression by

$$D_0 = \frac{c_2}{c_1} \tag{13}$$

and

$$B\sigma_{\mathrm{Rt}} = \frac{1}{\sqrt{c_2}}, \tag{14}$$

By including Eqs. (9)(13) and (14) in Eq. (10), K_{IQ} can be written as

$$K_{\mathrm{IQ}} = \frac{\sqrt{a\pi}}{\sqrt{c_2 + c_1 D}} f_1\left(\frac{a}{D}\right). \tag{15}$$

For large D, c_2 can be neglected in Eq. (15). According to Fig. 4 the specimen behaviour is linear elastic for large D, i.e. K_{IQ} tends to $K_{\mathrm{Ic}}^{\mathrm{e}}$, and Eq. (15) simplifies to

$$K_{\mathrm{Ic}}^{e} = \sqrt{\frac{\pi}{c_1}\left(\frac{a}{D}\right)} f_1\left(\frac{a}{D}\right) \quad \text{for } D \gg D_0. \tag{16}$$

4.3. Size correction based on FAD

Beyond LEFM, the fracture process is governed by the interaction of the stress intensity factors K_{I} and the global stresses σ_{Na} acting in the region of the crack tip. A practical tool to cope with this complex situation of an interaction of local and global stresses is the so-called failure assessment diagram (FAD), which represents the interaction as a failure line in the plane K_{I}–σ_{Na}, as schematically shown in Fig. 5 (Milne et al., 1988). FADs are often used to assess the stability of a cracked structural component in elastic-plastic fracture mechanics. Reversing the idea, the FAD might serve to estimate fracture toughness K_{Ic} from the apparent fracture toughness values K_{IQ} determined with specimens that did not fulfil the size requirement (Fig. 5). In Milne et al. (1988) a universal FAD was given as

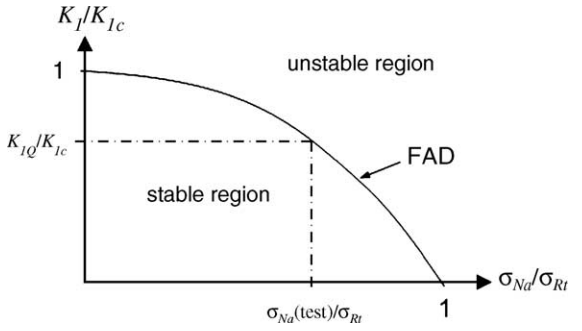

Fig. 5. Theoretical failure assessment diagram (FAD) for brittle material behaviour.

$$K_r = \frac{0.3 + 0.7\exp\left(-0.6L_r^6\right)}{\sqrt{1 + 0.5L_r^2}}. \tag{17}$$

In the terminology of the present paper, $K_{\mathrm{r}}=K_{\mathrm{IQ}}/K_{\mathrm{Ic}}$ and $L_{\mathrm{r}}=\sigma_{\mathrm{Na}}/\sigma_{\mathrm{Rt}}$.

The global stress σ_{Na} of a 3PB-specimen is similar to the nominal stress σ_{N} (Eq. (11)) of the remaining cross section $(h-a)$. Assuming for the sake of simplicity – as common in FAD-application – an ideal plastic stress distribution in the ligament, the elastic stress given by Eq. (11) is reduced by a factor of 2/3 (e.g. Nash, 1998), thus:

$$\sigma_{\mathrm{Na}} = \frac{1}{(h-a)^2}\left[\frac{F_c s}{w} + \frac{1}{2}\left(\frac{G_{\mathrm{3PB}}}{s}\right)\left[s^2 - (l-s)^2\right]\right]. \tag{18}$$

The analogous global stress for the CB-tests includes the shear stresses. Taking them into account roughly by applying Mohr's circle to the global stresses, one obtains:

$$\sigma_{\mathrm{Na}} = \frac{2M}{(h-a_c)^2} + \sqrt{\left(\frac{2M}{(h-a_c)^2}\right)^2 + \left(\frac{G_{\mathrm{CB}}}{h-a_c}\right)^2}. \tag{19}$$

However, being established semi-analytically for elastic-plastic materials, Eq. (17) is not expected to hold for snow as well without any restrictions. An alternative FAD derived on a theoretical basis in Schindler (2004) is

$$\frac{K_{\mathrm{IQ}}}{K_{\mathrm{Ic}}} = \sqrt{1 - \frac{\sigma_{\mathrm{Na}}}{C\sigma_{\mathrm{Rt}}}}. \tag{20}$$

Eq. (20) only holds for $R_{\mathrm{c}} \ll a$, but from experience in elastic-plastic fracture mechanics it is expected that the range of applicability of Eq. (20) exceeds the range of LEFM considerably. By evaluating Eqs. (17) or (20) K_{Ic} can be estimated from K_{IQ} values.

5. Results and discussion

During winter 2003/2004 five series of experiments were performed (Table 2). In the first two series (A, B) the specimens were tested in 3PB. Series C and D included 3PB-tests and CB-tests. In series E different specimen sizes were used.

5.1. Density dependence

The critical stress intensity factors (SIF), K_{IQ}, were evaluated for the 3PB-tests and CB-tests of series A–E, according to Eqs. (1) and (6), respectively. The results are compiled in Fig. 6 and Table 2. The dependence of mechanical properties on density can be described with a power–law relation (Perla et al., 1982):

$$K_{IQ} = A\rho^B. \quad (21)$$

The coefficients A and B were determined by using a log–log plot of the data presented in Fig. 6 and by applying a linear regression line. For series A–E this resulted in $A=(2.9\times10^{-6}\pm3.4\times10^{-6})$ kN m$^{3/2}$ kg^{-1} and $B=2.40\pm0.14$. The linear regression was statistically highly significant ($p<0.0001$). Schweizer et al. (2004) reported values for A between 3.1×10^{-5} kN m$^{3/2}$ kg^{-1} and 1.3×10^{-5} kN m$^{3/2}$ kg^{-1} and for B between 1.9 and 2.1 depending on snow type. For comparison, the relations fitted by Schweizer et al. (2004) for CB-tests are shown in Fig. 6.

The power–law fits suggested by Schweizer et al. (2004) given in Fig. 6 show that their K_{IQ} values were on average lower than the ones obtained in the present study. The difference is relatively small up to a density of about 250 kg/m^3 and further increases with increasing density. A comparison of the results with those of Schweizer et al. (2004) is difficult because their measurements are limited to densities up to 275 kg/m^3, whereas most of our measurements were with densities above 300 kg/m^3. The lack of sufficient data at low densities might have had an influence on the value of coefficient B which cannot be quantified. Furthermore, Eq. (6) can differ considerably from the one used by Schweizer et al. (2004). For deep cuts, K_{IQ} might be underestimated by their equation.

5.2. Shape dependence

According to LEFM, K_{IQ} should be a material constant and independent of the test method, i.e. equivalent to the fracture toughness K_{Ic}. However, the K_{IQ} values for the CB-tests in Fig. 6 tend to be significantly smaller than those for the 3PB-tests. Among the CB-tests, the ones with a cantilever length of $L=10$ cm failed at smaller K_{IQ} than the ones with $L=15$ cm. Hence, a dependence of K_{IQ} on the test method can be observed. The essential difference between the test methods is their different specimen shape (Fig. 2), since the effect due to mixed-mode fracture in the CB-tests was taken into account (Eq. (6)). Therefore, the geometry of the

Table 2
Summary of type and number of experiments (3PB: Three-point bending, CBT 10: Cantilever beam test with $L=10$ cm, CBT 15: Cantilever beam test with $L=15$ cm)

Series	Type and no. of experiments			Specimen sizes (h, l, w) (cm)	Snow type	Snow density (kg/m^3)	Snow temperature (°C)
	3PB	CBT 10	CBT 15				
A	7	–	–	(20, 50, 10)	Small rounded, 0.25–0.5 mm, 1F–	254 ± 12	−6.5
B	12	–	–	(20, 50, 10)	Decomposed and fragmented, partly faceted, 0.5–1 mm, F–4F	148 ± 3	−8.8
C	6	11	4	(20, 50, 10)	Small rounded and faceted, 0.25–0.75 mm, 4F	220 ± 7	−10.6
D	27	13	26	(20, 50, 10)	Small rounded and partly mixed forms, 0.5–1 mm, 1F–K	328 ± 17	−11.0
E	20	–	–	(8, 20, 10) (13, 31, 10) (20, 50, 10) (32 , 80, 10)	Decomposed and fragmented, small rounded, 0.5–1 mm, F–4F	186 ± 12	−14.5

Snow type is given as grain shape, grain size and hardness (hand test) according to ICSSG (Colbeck et al., 1990).

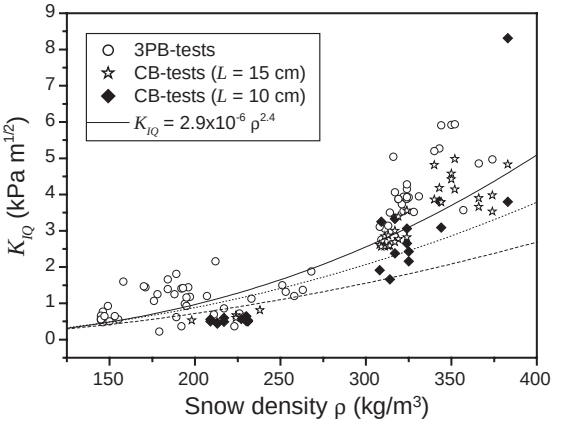

Fig. 6. Critical SIF in relation to density (series A–E). The data is distinguished according to the test method used. The power–law fit is based on a linear regression in a log–log plot. For comparison the power–law fits by Schweizer et al. (2004) are added; $K_{IQ}=3.1\times10^{-5}\rho^{1.9}$ (dashed line) and $K_{IQ}=1.3\times10^{-5}\rho^{2.1}$ (dotted line).

specimens seems to be responsible for the difference. This effect has been previously described by Faillettaz et al. (2002) and Schweizer et al. (2004).

Fig. 7 shows the critical SIF, K_{IQ}, in relation to the relative notch length (a/h) for series D. In order to eliminate the density dependence the data were normalised to a density of 330 kg/m^3, which was approximately the mean density of series D ($\rho=328\pm17$ kg/m^3). This was made by assuming a linear relation between density and K_{IQ}, what is justified for a limited density range.

The mean K_{IQ} for the 3PB-tests (4.2 kPa m$^{1/2}$) was 24% larger than the mean for the CB-tests (3.4 kPa m$^{1/2}$). This corresponds to the findings in Fig. 6. In Fig. 7 it can be seen that for the CB-tests K_{IQ} increased with increasing cantilever length L. This supports the assumption of a shape effect. A shape effect has to be expected if LEFM does not apply. For the cantilever beam tests K_{IQ} was increasing with increasing notch length to specimen height ratio (a/h). This corresponds to the findings of Schindler (1996) for small ceramic specimens.

5.3. Fracture process zone

If the tensile strength σ_{Rt} and the fracture toughness K_{Ic} are known, the size of the fracture process zone R_c can be estimated by Eq. (8). Because we do not have yet a suitable size correction to extract K_{Ic} from measurements of K_{IQ}, we used K_{IQ} to estimate R_c according to Section 3. Since no direct measurements of the tensile strength were made, it was estimated from the nominal stress for each measurement according to Eqs. (18) and (19) (Fig. 8). For a given density one can assume that the measured nominal stresses of the notched specimens have to be smaller than the nominal stress of the unnotched specimens, which would correspond to the tensile strength. Therefore, a power–law relation with the boundary condition $\sigma_{Rb}(\rho=0)=0$ was fitted to the data in Fig. 8 such that it formed an upper boundary: $\sigma_{Rb}=1.23\times10^{-4}\ \rho^{2.1}$ kPa. The estimated tensile strength σ_{Rb} was comparable to previous measurements found in the literature. For example, for a density of 200 kg/m^3 we estimated a tensile strength of about 8.4 kPa. According to measurements summarized by Mellor (1975) the tensile strength is about 2–10 kPa. Jamieson and Johnston (1990) found lower values of about 2 kPa.

With the estimate of the tensile strength and the use of Eq. (8) the size of the process zone is plotted in Fig. 9 as a function of snow density. For a typical snow slab avalanche density of about 180 kg/m^3, R_c is about 1.1 cm.

Since we used K_{IQ} instead of K_{Ic}, the resulting R_c values represent a lower boundary of the effective size of the fracture process zone. Thus, the

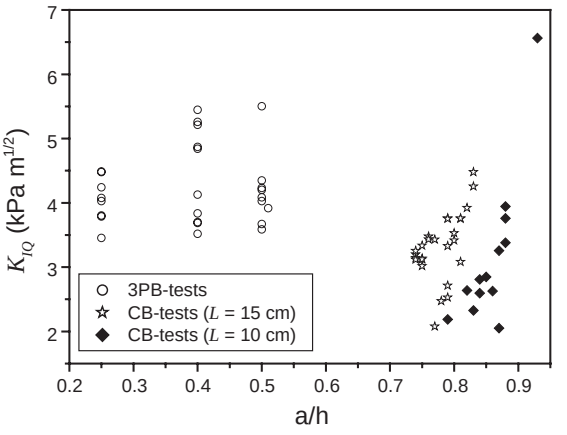

Fig. 7. Comparison of 3PB-tests and CB-tests (Series D). Critical SIF in tension in relation to the relative notch length (a/h). The results were normalised to a density of 330 kg/m^3.

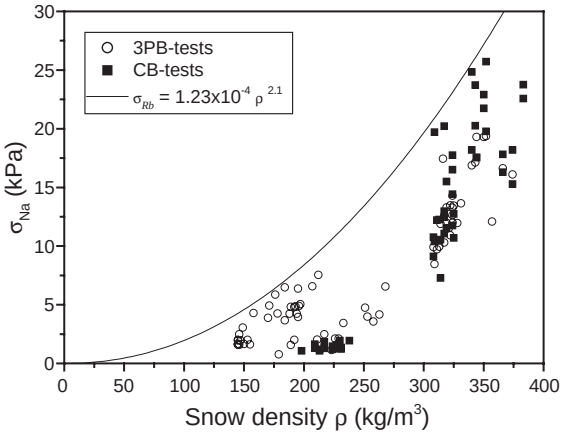

Fig. 8. Estimate for the tensile strength in bending σ_{Rb} as the upper boundary of the nominal stress values σ_{Na}.

fracture process zone R_c was larger than, $a/8$ or $(a-h)/8$, the limits for LEFM (cf. Section 3) for most of our experiments. The fracture behaviour of a non-ductile material due to a relatively large fracture process zone is often called "quasi-brittle" (Bazant and Planas, 1998).

5.4. Size dependence

Results of fracture experiments with four different specimen sizes (series E) are shown in Fig. 10. The ratio of notch length to specimen height (a/h) was kept constant at 1/10. In Fig. 10a K_{IQ} is plotted in relation to the specimen height h. K_{IQ} increased with increasing specimen size. A linear regression was statistically significant ($p=0.003$) with a slope of -1.9 ± 0.5. In Fig. 10b the data are shown in a log–log plot as in Fig. 4. The nominal strength σ_N decreased with increasing specimen size. The decrease was statistically significant ($p=0.003$) with a slope of -0.23 ± 0.07.

D_0, $B\sigma_{Rt}$ can be evaluated by a linear regression of the data if $(1/\sigma_N^2)$ is plotted vs. sample height h (Eqs. (12)–(14)). The linear regression yields 0.07 ± 0.02 kPa^{-2} m^{-1} for the slope and 0.02 ± 0.01 kPa^{-2} for the intercept with a level of significance of $p=0.015$.

$$D_0 = 0.30\pm0.13\,\mathrm{m}$$

$$B\sigma_T = 7.07\pm0.88\,\mathrm{kPa}$$

With Eq. (16) and $(a/D)=1/10=$const., K_{Ic}^e can be determined:

$$K_{Ic}^e = 2.20\pm0.40\ \mathrm{kPa}\sqrt{\mathrm{m}}.$$

The slope in Fig. 10b is less than $-1/2$, as associated with LEFM in Fig. 4. The slope (-0.23) indicates that specimen sizes were in the range of D_0 in Fig. 4. This suggests that our specimens were not large enough to be in a range where LEFM would be applicable. The reason for this is the large size of the fracture process zone. However, it is hardly possible to increase the sample size because larger samples cannot be handled any more.

The equivalent fracture toughness $K_{Ic}^e=2.20\pm0.40$ kPa m$^{1/2}$ was as expected larger than the value obtained by the power–law fit of Eq. (21) of $K_{IQ}=0.81$ kPa m$^{1/2}$, with $A=2.9\times10^{-6}$ kN m$^{3/2}$ kg^{-1}, $B=2.4$ and a density of 186 kg/m^3. The effectively measured mean K_{IQ} of series E was about 1.2 kPa m$^{1/2}$.

The ratio $\beta=D/D_0$ should be at least 25 if the deviation from LEFM should be less than 2% (Bazant and Planas, 1998). At best we obtain a ratio of $\beta\approx1$, because D_0 is similar to our specimen dimensions. Thus, even the most optimistic estimates indicate that the specimen dimensions required for LEFM are too large for any practical purpose. Even in the case of a snow slab avalanche this criterion is not fulfilled. Fracture depths mea-

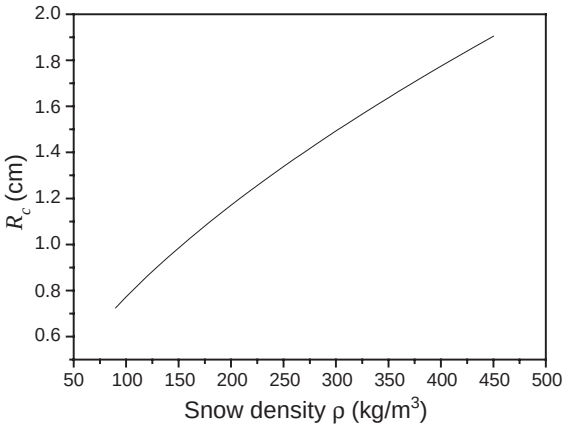

Fig. 9. Size of fracture process zone R_c in relation to snow density derived from K_{IQ} and σ_{Rb} values.

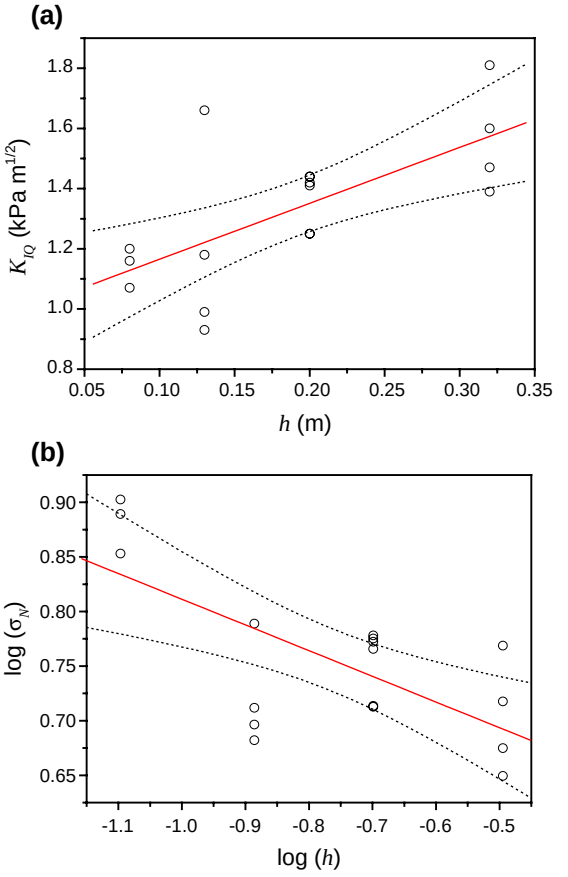

Fig. 10. Tests with four different specimen sizes (series E). Three out of 20 measurements had to be excluded due to failure during preparation. Snow density was 186 ± 12 kg/m^3. (a) Critical SIF K_{IQ} vs. specimen height h. (b) Nominal strength σ_N vs. specimen height h in a log–log plot. The dashed lines indicate the 95% confidence band of the linear regression.

sured slope perpendicular at the crown (tensile fracture) of slab avalanches were about 65 cm for a dataset including natural and human triggers (Perla, 1977) and about 40 cm for only human-triggered avalanches (Schweizer and Lütschg, 2001). Eq. (15) can be used for a first estimate of a critical stress intensity value representative for a slab thickness $D = 50$ cm

$$K_{IQ}^{slab} = 1.69\,\mathrm{kPa}\sqrt{\mathrm{m}}.$$

The ratio (a/D) was kept at 1/10 as for the experiments. For future estimates of K_{Ic}^{slab} a shape correction has to be added accounting for the different shapes between laboratory experiments and slab geometry.

The above results are only a rough estimate and have to be considered as preliminary because of the small number of experiments, ($N = 20$) out of which 3 had to be excluded because the specimens failed during preparation. Therefore, further experiments and an increased measurement precision will be needed to corroborate these findings.

5.5. FAD determination

By the correction based on Eqs. (17) or (20) no tendency of convergence to a size-independent K_{Ic} value was found. This indicates that the actual FAD for the present material and specimen geometry differs significantly from the ones described by Eqs. (17) or (20). To obtain an improved, test-specific FAD, the experimental data have to be plotted in a diagram ($\sigma_{Na}/C\sigma_{Rb}$) vs. (K_{IQ}/K_{Ic}). In order to normalize both axes, the tensile strength σ_{Rb} and the fracture toughness K_{Ic} had to be estimated. To estimate σ_{Rb} the power law relation (Fig. 8) was used. To estimate K_{Ic}, K_{IQ} was plotted in relation to ($\sigma_{Na}/C\sigma_{Rb}$) with C set to 1. Theoretically K_{IQ}/K_{Ic} should be about one for $\sigma_{Na}/C\sigma_{Rb} < 0.3$. Therefore, K_{Ic} was estimated as the upper boundary of the K_{IQ} values for which $\sigma_{Na}/C\sigma_{Rb} < 0.3$. The corresponding experimental data are shown in Fig. 11. As an FAD two linear

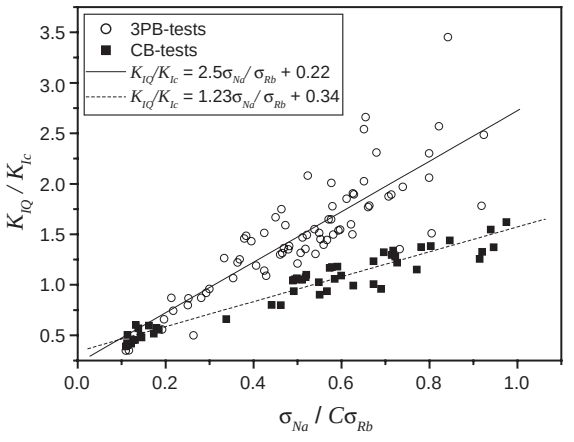

Fig. 11. Failure Assessment Diagram (FAD) for series A–E. The coefficient C (Eq. (20)) was set to 1.

regression lines for the two different test methods can be used:

3PB-specimens:

$$\frac{K_{IQ}}{K_{Ic}} = 2.5\frac{\sigma_{Na}}{\sigma_{Rb}} + 0.22 \quad (22)$$

CB-specimens:

$$\frac{K_{IQ}}{K_{Ic}} = 1.23\frac{\sigma_{Na}}{\sigma_{Rb}} + 0.34. \quad (23)$$

Although the values seem to correlate well, especially for the CB-tests, Eqs. (22) and (23) do not resemble the typical shape of an FAD (Fig. 5), which is characterized by a decreasing K_r with increasing L_r as described by Eqs. (17) and (20). This behaviour cannot be explained so far and requires further investigations. Reasons for the differing shapes of Figs. 5 and 11 might be that the condition behind Eq. (20), $R_c \ll a$, was not fulfilled for our experiments and that the outcome of Fig. 11 is very sensitive on how the upper boundaries to estimate σ_{Rb} and K_{Ic} are chosen. The latter reason concerns rather the scatter of the points than the influence on the slope of a linear regression. Measuring the tensile strength σ_{Rb} in parallel to the toughness might decrease the uncertainties when applying this method.

Eqs. (22) and (23) can be used at least formally to correct the K_{IQ} values according to Section 4.3. The resulting K_{IQ} values are shown in Fig. 12. The calculated K_{Ic} values now converge compared to the K_{IQ} values, not only between the different sizes but also between the two specimen types, at least for higher snow densities.

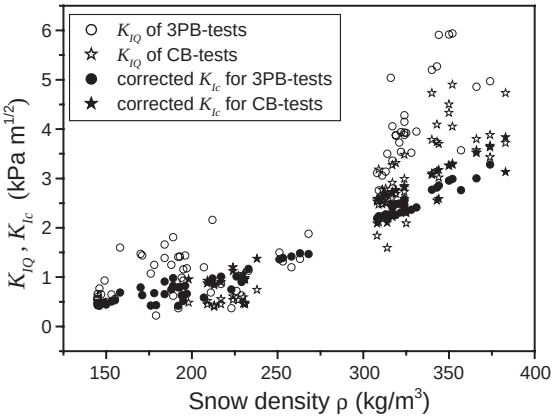

Fig. 12. K_{IQ} values in comparison to the corresponding corrected K_{Ic} values for 3PB and CB-tests.

The absolute value of K_{Ic} can not be considered as being representative at the moment, because of the rough estimate of σ_{Rb} and K_{Ic} to normalize the axis as mentioned above and the problems in explaining the increasing K_r with increasing L_r.

6. Conclusions

In order to investigate the size and shape-dependence of fracture toughness measurements on laboratory-sized specimens of snow, tests with three different specimen geometries and four different sizes were performed. The three specimen geometries consisted of a three-point bending test and two cantilever beam tests with cantilever lengths of 10 cm and of 15 cm. The 3PB-test method was adapted to snow experiments for the first time and proved to be applicable.

The critical stress intensity factors found were similar to previous measurements, with a similar density dependence. The 3PB-tests provided higher values than the CB-tests which depended on cantilever length. The differences between the test methods were significant and attributed to non-negligible size and shape effects. The fracture process zone was estimated to be in the order of at least one centimetre, implying that snow has to be considered as a quasi-brittle material at the scale of our experiments. For a quasi-brittle material linear elastic fracture mechanics (LEFM) is applicable only with a size correction.

As a method to correct the apparent fracture toughness to the size-independent material property K_{Ic} the equivalent fracture toughness according to Bazant and Planas (1998) was determined. Preliminary results suggest that the actual fracture toughness K_{Ic} can be twice as large as the apparent one in the experiments. From the present results, fracture toughness is expected to be size dependent up to the scale of a slab avalanche. Therefore, an appropriate scaling law for K_{Ic} is essential when fracture mechanics is applied to predict avalanche release.

As a possibility to correct individual toughness data from laboratory specimens, a new method based on the FAD-theory was explored. For this purpose the specific FAD for a certain test method had to be established by a

series of tests, since the universal FADs given in the literature were found to be inadequate for the present purpose. The preliminary results are promising, but the obtained FADs have to be considered as tentative and have to be verified by further tests.

The presented results represent some first steps aimed at designing laboratory measurements to determine snow fracture toughness which will be transferable to snow slope stability and avalanche release modelling.

Acknowledgements

We thank David McClung for useful discussions and constructive comments and Nora Staack and Ruzica Dadic for help with the experiments.

References

Anderson, T.L., 1995. Fracture Mechanics: Fundamentals and Applications. CRC Press, Boca Raton, U.S.A. 688 pp.

Barenblatt, G.I., 1962. The mathematical theory of equilibrium cracks in brittle fracture. Adv. Appl. Mech. 7, 55–129.

Bazant, Z.P., Planas, J., 1998. Fracture and Size Effect in Concrete and other Quasibrittle Materials. CRC Press, Boca Raton, U.S.A. 616 pp.

Bazant, Z.P., Zi, G., McClung, D., 2003. Size effect law and fracture mechanics of the triggering of dry snow slab avalanches. J. Geophys. Res. 108 (B2), 2119.

Colbeck, S.C., et al., 1990. The international classification of seasonal snow on the ground, International Commission on Snow and Ice (ICSI). International Association of Scientific Hydrology, Wallingford. 23 pp.

Dempsey, J.P., Adamson, R.M., Mulmule, S.V., 1999a. Scale effects on the in-situ tensile strength and fracture of ice: Part II. First-year sea ice at Resolute, N.W.T.. International Journal of Fracture 95, 347–366.

Dempsey, J.P., Defranco, S.J., Adamson, R.M., Mulmule, S.V., 1999b. Scale effects on the in-situ tensile strength and fracture of ice: Part I. Large grained freshwater ice at Spray Lakes Reservoir, Alberta. International Journal of Fracture 95, 325–345.

Erdogan, F., Sih, G.C., 1963. On the crack extension in plates under plane loading and transverse shear. J. Basic Eng. 85, 519–527.

Faillettaz, J., Daudon, D., Bonjean, D., Louchet, F., 2002. Snow toughness measurements and possible applications to avalanche triggering. In: Stevens, J.R. (Ed.), Proceedings ISSW 2002. International Snow Science Workshop, Penticton BC, Canada, 29 September–4 October 2002, pp. 540–543.

Irwin, G.R., 1958. Fracture. Handbuch der Physik. Springer-Verlag, Berlin, pp. 551–590.

Jamieson, J.B., Johnston, C.D., 1990. In-situ tensile tests of snowpack layers. J. Glaciol. 36 (122), 102–106.

Kirchner, H.O.K., Michot, G., Suzuki, T., 2000. Fracture toughness of snow in tension. Philosophical Magazine. A 80 (5), 1265–1272.

Kirchner, H.O.K., Michot, G., Schweizer, J., 2002a. Fracture toughness of snow in shear and tension. Scripta Materialia 46 (6), 425–429.

Kirchner, H.O.K., Michot, G., Schweizer, J., 2002b. Fracture toughness of snow in shear under friction. Phys. Rev., E 66 (2) (027103(3)).

McClung, D.M., 1981. Fracture mechanical models of dry slab avalanche release. J. Geophys. Res. 86 (B11), 10783–10790.

Mellor, M., 1975. A review of basic snow mechanics. IAHS-AISH Publication 114, 251–291.

Milne, I., Ainsworth, R.A., Dowling, A.R., Stewart, A.T., 1988. Assessment of the integrity of structures containing defects. Int. J. Press. Vessels Piping 32 (1–4), 3–104.

Nash, W.A., 1998. Schaum's Outline of Theory and Problems of Strength of Materials. McGraw-Hill, New York, U.S.A. 474 pp.

Perla, R., 1977. Slab avalanche measurements. Can. Geotech. J. 14 (2), 206–213.

Perla, R., LaChapelle, E.R., 1970. A theory of snow slab failure. J. Geophys. Res. 75 (36), 7619–7627.

Perla, R., Beck, T.M.H., Cheng, T.T., 1982. The shear strength index of alpine snow. Cold Reg. Sci. Technol. 6 (1), 11–20.

Schindler, H.J., 1996. Size effects on fracture toughness of brittle materials. International Journal of Fracture 82, R3–R10.

Schindler, H.J., 2004. Grundlagen der Bruchmechanik, Lecture Notes. ETH, Zürich.

Schweizer, J., Lütschg, M., 2001. Characteristics of human-triggered avalanches. Cold Reg. Sci. Technol. 33 (2–3), 147–162.

Schweizer, J., Jamieson, J.B., Schneebeli, M., 2003. Snow slab avalanche formation. Reviews of Geophysics 41 (4), 1016.

Schweizer, J., Michot, G. and Kirchner, H.O.K., 2004. On the fracture toughness of snow. Ann. Glaciol., 38, 1–8.

Tada, H., Paris, P.C., Irwin, G.R., 2000. The Stress Analysis of Cracks Handbook. ASME Press, New York. 696 pp.